Smart Structures and Systems, *Vol. 26, No. 3 (2020) 277-290*
DOI: https://doi.org/10.12989/sss.2020.26.3.277

Ground surface changes detection using interferometric synthetic aperture radar

Loke Kok Foong [1,2a], Ali Jamali [3b] and Zongjie Lyu*[4,5]

[1] *Department for Management of Science and Technology Development, Ton Duc Thang University, Ho Chi Minh City, Vietnam*
[2] *Faculty of Civil Engineering, Ton Duc Thang University, Ho Chi Minh City, Vietnam*
[3] *Faculty of Surveying Engineering, Apadana Institute of Higher Education, Shiraz, Iran*
[4] *Institute of Research and Development, Duy Tan University, Da Nang 550000, Vietnam*
[5] *Faculty of Civil Engineering, Duy Tan University, Da Nang 550000, Vietnam*

(*Received December 15, 2019, Revised February 22, 2020, Accepted June 6, 2020*)

Abstract. Disasters, including earthquakes and landslides, have enormous economic and social losses besides their impact on environmental disruption. Iran, and particularly its Western part, is known as an earthquake susceptible area due to numerous strong ground motions. Studying ecological changes due to climate change can improve the public and expert sector's awareness and response to future disastrous events. Synthetic Aperture Radar (SAR) data and Interferometric Synthetic Aperture Radar (InSAR) technologies are appropriate tools for modeling and surface deformation modeling. This paper proposes an efficient approach to detect ground deformation changes using Sentinel-1A. The focal point of this research is to map the ground surface deformation modeling is presented using InSAR technology over Sarpol-e Zahab on 25th November 2018 as a study case. For surface deformation modeling and detection of the ground movement due to earthquake SARPROZ in MATLAB programming language is used and discussed. Results show that there is a general ground movement due to the Sarpol-e Zahab earthquake between -7 millimeter to +18 millimeter in the study area. This research verified previous researches on the advanced image analysis techniques employed for mapping ground movement, where InSAR provides a reliable tool for assisting engineers and the decision-maker in choosing proper policies in a time of disasters. Based on the result, 574 out of 682 damaged buildings and infrastructures due to the 2017 Sarpol-e Zahab earthquake have moved from -2 to +17 mm due to the 2018 earthquake with a magnitude of 6.3 Richter. Results show that mountainous areas have suffered land subsidence, where urban areas had land uplift.

Keywords: sentinel; SAR; InSAR; forest; disaster monitoring; earthquake

1. Introduction

As a widespread disaster, massive mass movements like landslides are known as a disastrous natural hazard (Moayedi *et al*. 2019a, c, Kallel *et al*. 2019, Nguyen *et al*. 2019). However, these events usually occur in the local and regional scales; they can bring severe damages and life losses on a national level (Bui *et al*. 2019b, c, Moayedi *et al*. 2019d, Van Dao *et al*. 2020). Various phenomena and human-made infrastructures such as roads, dams, residential buildings, etc. can be damaged by such events (Moayedi *et al*. 2011, 2019b, Zhu *et al*. 2012, Zhang *et al*. 2016, Yuan and Moayedi 2019a, b). In China, for example, landslides and floods featured as the second dangerous economic disaster between May and August 2010 due to US$ 18 billion worth of damage (Guha-Sapir *et al*. 2012). Accordingly, massive mass movements have killed 1,765 people to be one of the ten most crucial catastrophes in the case of psychological damages (Choi *et al*. 2011, Guha Sapir *et al*. 2012, Mei 2017). A large area can be affected by landslide causative events like earthquakes, typhoons, rainfalls, etc. In Taiwan, as a susceptible area, for instance, Typhoon Morakot (i.e., in 2009) triggered more than 9,000 landslides Tsai and Chen (2010).

Considering the reported damages (i.e., both financial and psychological damages) and the importance of the issue of slope stability (Bui *et al*. 2019a, Moayedi *et al*. 2019e, Liu *et al*. 2020, Wang *et al*. 2020), the development of reliable, fast, and inexpensive models for mapping and interpreting earth observation is more and more highlighted. In the particular case of landslides, providing the landslide inventory map plays an essential role in many relevant risk analyses. Traditional manners that have been used for deriving landslide locations are field monitoring (e.g., using GPS) and aerial photo interpretations. Such methods, however, offer exact results, they are significantly the time and cost consuming. As well as this, scholars may encounter problems for doing field surveys in inaccessible sites. Satellite imagery yields a simply-performed way of monitoring and detecting landslides in every susceptible area. Remarkably, the growing trend of the spatial resolution of this technology enables us to obtain more accurate results (e.g., Debella-Gilo and Kääb (2012), and Stumpf and Kerle (2011)). Application of remote sensing methods such as satellite and airborne imagery and

*Corresponding author, M.Sc.,
E-mail: zongjielyu@duytan.edu.vn
[a] Ph.D., E-mail: lokekokfoong@tdtu.edu.vn
[b] Ph.D., E-mail: ali.jamali.65@gmail.com

ISSN: 1738-1584 (Print), 1738-1991 (Online)

altimetry has raised for various investigations like river hydrodynamics, floodplain inundation, and floods (Schumann 2017). There are many numbers of sensors and data processing techniques to analyze and process information (Ebrahimi *et al*. 2016, Baziar and Rostami 2017, Rostami *et al*. 2018, Kargar *et al*. 2020). For instance, sensors that record flood phenomena are in the visible, microwave, and thermal range of the electromagnetic spectrum.

For surface deformation measuring due to geo-hazards including earthquakes, landslides, and floods, Spaceborne interferometric synthetic aperture radar (InSAR) a technique that uses the high spatial resolution and remotely-acquired data Ferretti *et al*. (1999) and Hooper (2008) has been used. The name (InSAR) symbolizes a potent technique that enjoys the high spatial resolution and remotely-acquired data for assessing surface deformation caused by geo-hazards, including earthquakes, landslides, and floods (Hooper 2008). Numerous mathematical based solutions are proposed to solve complex engineering problems (Liu *et al*. 2020, Qiao *et al*. 2019a, b, Qiao and Yang 2019a, b, Zhang *et al*. 2019b, Chen *et al*. 2020, Jinlong *et al*. 2020, Zhou *et al*. 2020a, b). At the same time, satellite imageries of the land surface provide full information of geomorphometry on landforms (Glenn *et al*. 2006, Hugenholtz *et al*. 2013). Radar sensors have provided valuable information about the near-surface landforms. Note that this information plays a complementary role in visible and infrared sensors. Today, Interferometric Synthetic Aperture Radar (InSAR) is a valuable tool for measuring surface deformations induced by earthquakes (Ambrosi, Strozzi, Scapozza, & Wegmüller, 2018; Qu, Zuo, Shan, Hu, & Zhang, 2017). This tool has been effectively applied to understanding and quantification of co- seismic (Barnhart *et al*. 2018), inter-seismic strain (Karimzadeh *et al*. 2013), and post-seismic (Montecino *et al*. 2017) associated with large earthquakes. It has been demonstrated that InSAR keeps its sensitivity to displacements and deformations triggered by moderate to small magnitude earthquakes (Dicelis *et al*. 2016, He *et al*. 2018, Farolfi *et al*. 2019).

Accordingly, as significant landslides occurrence is connected to a massive earthquake thus is challenging to foresee. Many scientists used SAR data related to before and after earthquakes to detection the corresponding deformations by earthquakes (Valerio *et al*. 2018). SAR interferometry is a practical tool for detecting land deformations caused by earthquakes (Chen *et al*. 2014), as well as for estimation of glacier surface motion (Dai *et al*. 2016); application of Differential InSAR (DInSAR) techniques to measure the seasonal (Fang *et al*. 2016) and multi-year surface displacements studies has been the subject of a few works in recent times. InSAR allows us to have a reliable mapping from surface deformation at an unprecedented spatial resolution (Wright *et al*. 2004). Creating time-series data provides a beneficial way to assess the temporal behavior of the identified phenomena. It also enables us to investigate the evolution of the proposed deformations (Berardino *et al*. 2002).

InSAR based Surface deformation for Taiwan by the Small Baseline Subset (SBAS) method from April 2016 to April 2017 was investigated by Yang *et al*. (2019). For surface deformation modeling, they used Global Positioning System (GPS) and InSAR by reducing velocity difference between InSAR derived displacement and GPS measurement. In their study, combined measurements from InSAR and GPS showed that dry-season land subsidence was from 60 percent to 74 percent of the total land subsidence. The InSAR technique was considered as an effective method for land subsidence modeling in their research. Time series InSAR based deformation monitoring for land subsidence in Xi'an, China, was researched by Wang *et al*. (2019) from 20 June 2015 to 17 July 2019. They concluded that from multi-temporal InSAR techniques, time-series deformation could be derived to model the temporal evolution of land subsidence in Xi'an, China. For the estimation of an interferometric component related to displacement, the SBAS technique should be predefined on a deformation model where differential SAR interferometry (DInSAR) method does not have this limitation (it does any need any deformation model). On the other hand, the DInSAR process has a limited accuracy compared to SBAS technique caused from temporal and spatial decorrelation, atmospheric signal delay, and orbital/topographic errors (Pawluszek-Filipiak and Borkowski 2020). As a result, Pawluszek-Filipiak and Borkowski (2020) used the integration of SBAS and DInSAR techniques for mining-related deformations using Sentinel-1 data. In their study, a Kriging-based integration method of DInSAR and SBAS could effectively be used for mining-related land subsidence monitoring.

Du *et al*. (2020) used SBAS and Temporarily coherent point (TCP) InSAR techniques as two current multi-temporal interferometric synthetic aperture radar (MTInSAR) technique for land subsidence along with the coastal areas of Guangdong, China. They used long-wavelength L-band ALOS/PALSAR-1 dataset from 2007 to 2011. They concluded that aquaculture regions suffered 40.8 percentage of the total land subsidence, followed by urban, agricultural, and forest regions with 37.1, 21.5, and 0.6 percentages. Their results showed that groundwater exploitation for aquaculture and agriculture was probably the main reason for land subsidence in the region of study. Detection of active slope deformation analysis with the use of Sentinel-1 data in the Southwest Area of Shanxi, Chin was investigated by Shi *et al*. (2020). To model the unstable areas in Xiangning County, the time series InSAR analysis method was used in their research. They detected 597 unstable sites in a 41.7 km^2 area, where 70 percent of the identified sites that are prone to landslide is located in mountainous regions correlated with precipitation rate in the study area.

Overall, despite the fact that SAR data (i.e., Sentinel-1 SAR C-band data) are free and easy to access for the study areas, to the best knowledge of authors, no such attempt has been performed for displacement mapping after 2018 Sarpol-e Zahab earthquake. This results in limited state-of-the-art data on ground movement using remotely sensed information, particularly in the chosen study area. Also, InSAR techniques can satisfactorily deal with high

dimensionality issues. However, datasets can be handled by this method for displacement modeling. To date, the study has evaluated the applicability of the InSAR method for ground movement mapping is still rare in the study area for the 2018 earthquake. Hence, this work aims to fill the gap by applying InSAR techniques to map displacement model using the Sentinel-1 C-band data in Sarpol-e Zahab located on the north of Zahab plain, Iran after 2018 Sarpol-e Zahab earthquake.

2. Material and methods

2.1 Description of the study area and earthquake event

On Sunday night of 25th November 2018, the Sarpol-e Zahab earthquake with a magnitude of 6.3 Richter hit western of Iran at 20:07 local time, injuring over 700 people. The studied area is the Sarpol-e Zahab county located in the north of Zahab plain in Kermanshah province, Iran (Fig. 1). The coordinates of this area are 34°18′51″N 47°03′54″E. About Kermanshah, the average altitude is 1,350 m (4,430 ft) upper than sea level. Its population has been reported as 851,405 people in 2011. The presence of the Zagros mountains dramatically influences the climate of this province, which is chiefly categorized as the hot-summer Mediterranean. In general view, the Zagros structural domain is located in the central portion of the Arabia-Eurasia young collision zone (e.g., Berberian (1995), Agard *et al*. (2005), and Oveisi *et al*. (2009)). A relatively high elevation and being exposed to western winds brings high annual precipitation for Kermanshah in fall and spring. Because of the same reason, the daily air temperature is high indeed, especially during the rainless summers.

The Sarpol-e Zahab (see Fig. 2) is located in the Kermanshah province of Iran, which is situated in the north of Zahab plain with the annual average rainfall of the area is around 440 mm. August and September are considered as the hottest months with a maximum temperature of 41°C, where January is the coldest one with a minimum temperature of -2.5°C. The Sarpol-e Zahab was effected massively due to the 2017 earthquake with over 1000 injured and casualty with more than 14000 damaged buildings and infrastructures in the region.

Fig. 2 The study area (Sarpol-e Zahab) in Google Earth Pro

2.2 Synthetic aperture radar

Six Single Looks Complex (SLC) of Sentinel 1A images for displacement modeling using InSAR technology using SARPROZ (Perissin 2019) in MATLAB programming language are used. Properties of utilized Sentinel 1-A SLC images for the Sarpol-e Zahab earthquake is shown in Table 1. For various mapping aims such as providing a map of soil, agriculture, water, forests, emergency mapping support for natural disasters including flooding, landslide, earthquakes, Sentinel 1A, 1B satellites were launched. A C-SAR sensor is carried by Sentinel 1 satellites which give medium and high-resolution images. Notably, it can work in all weather conditions. The C-SAR is a powerful monitoring tool for both land and sea. It helps us to obtain night imagery and detects millimeter movements on the ground (Zhang *et al*. (2019a).

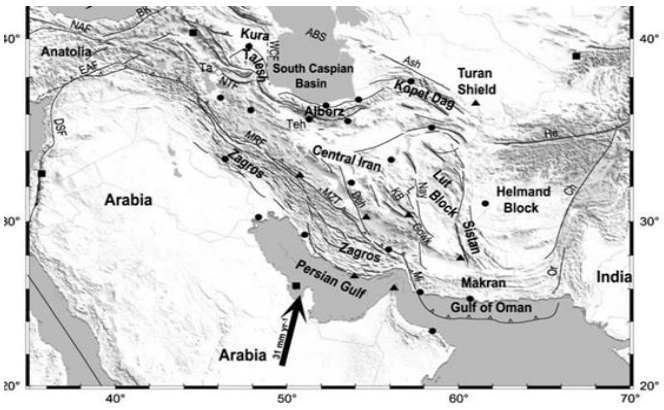

(a)

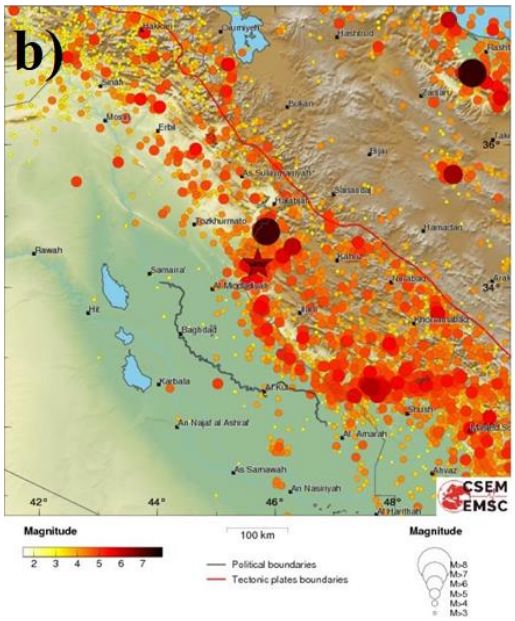

(b)

Fig. 1 (a) Simplified tectonic sehpgtting of Iran (Vernant *et al*. 2004); (b) Regional instrumental seismicity of 2018 Sarpol-e Zahab earthquake from CSEM/EMSC

Table 1 Single Look Complex (SLC) of Sentinel-1A images properties of the study area

Granule SLC name	Orbit	Acquisition mode	Acquisition date	Pass
S1A_IW_SLC__1SDV_20180903T025354_20180903T025421_023528_028FD9_2548	23528	Interferometric Wide Swath	03-09-2018	Descending
S1A_IW_SLC__1SDV_20180927T025354_20180927T025421_023878_029B21_0F68	23878	Interferometric Wide Swath	27-09-2018	Descending
S1A_IW_SLC__1SDV_20181009T025355_20181009T025422_024053_02A0E4_DD63	24053	Interferometric Wide Swath	09-10-2018	Descending
S1A_IW_SLC__1SDV_20181102T025355_20181102T025422_024403_02AC58_2387	24403	Interferometric Wide Swath	02-11-2018	Descending
S1A_IW_SLC__1SDV_20181126T025354_20181126T025421_024753_02B932_2387	24753	Interferometric Wide Swath	26-11-2018	Descending
S1A_IW_SLC__1SDV_20181220T025353_20181220T025420_025103_02C562_21B5	25103	Interferometric Wide Swath	20-12-2018	Descending

2.3 Data processing

As shown in Fig. 3, for displacement modeling using InSAR technology, first, the master image belonging to 2nd November 2018 (before the earthquake) is co-registered with slave image belonging to 26th November 2018 (after the quake) (see Fig. 4(a)). Co-registration guarantees that each ground target is related to the same (range, azimuth) pixel in both the slave and the master images. A pixel-to-pixel match between common features in SAR master and slave images is required for SAR interferometry. In a vital process for the final phase difference identification and noise reduction, the alignments of SAR images from two antennas (the co-registration) is needed. For exceptional InSAR results, a subpixel-to-subpixel match called co-registration is a must (Li and Bethel 2008). The coherence image (see Fig. 4(b)) is produced after two images are co-registered. Coherence is correlated with scatters between the two interfering SAR images (master and slave), and it is typically calculated by testing the phase variance (0 and 1) of pixels within a spatial window. It decreases with the physical changes/movement of the scatters, such as rockfall and landslide phenomena. Vital information to detect any mass movement or surface change can be extracted from InSAR coherence. Using radar intensity and phase differences from two SAR images in a different period, coherence change detection can be used. For land surface deformation monitoring caused by an earthquake, the coherence product of InSAR can be used, which is a sensitive and powerful tool. Coherence between the two images can be estimated by Eq. (1) (after both Master and Slave images are co-registered)

$$\gamma = \frac{\left|\sum_{r=0}^{R-1}\sum_{c=0}^{C-1} I_1(r.c)I_2^*(r.c)\right|}{\left\{\sum_{r=0}^{R-1}\sum_{c=0}^{C-1} |I_1(r.c)|^2 \sum_{r=0}^{R-1}\sum_{c=0}^{C-1} |I_2(r.c)|^2\right\}^{\frac{1}{2}}}. \quad 0 \le \gamma \le 1$$

Where γ is the absolute value of the coherence at a certain pixel, I_1 and I_2 are the two co-registered complex

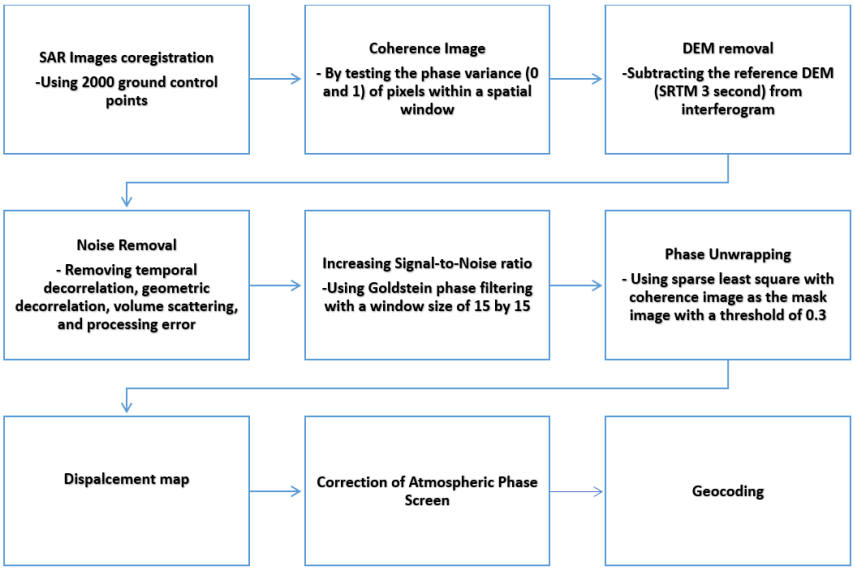

Fig. 3 Workflow chart for displacement modeling caused by the Sarpol-e Zahab earthquake

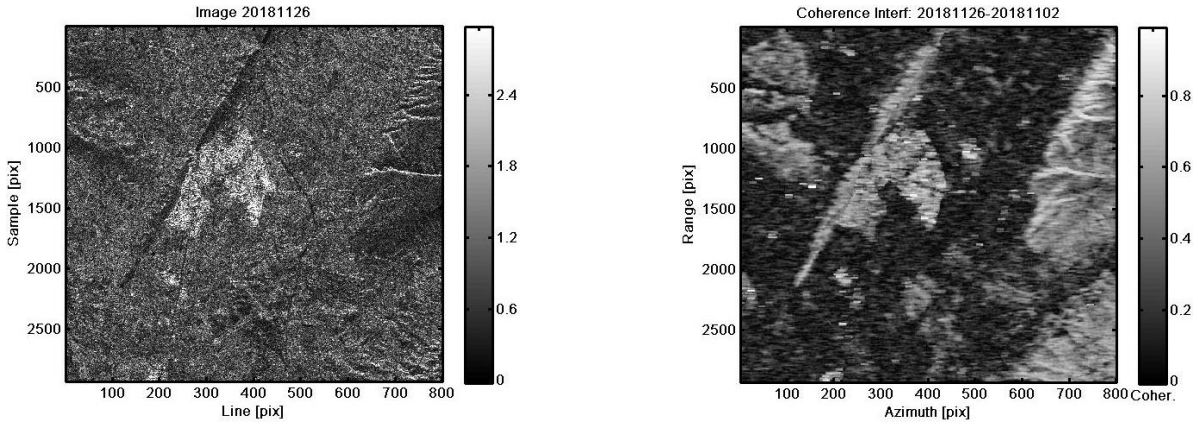

(a) (b)

Fig. 4 (a) Co-registered (left image); (b) coherence (right image) of surface deformation after the earthquake occurred in Sarpol-e Zahab on 25th November 2018 processed in SARPROZ in MATLAB

images ($I_1 =$ Master and $I_2 =$ Slave), and I_2^* is the complex conjugate of the other image. The coherence (γ) has values ranging between 0 and 1.

3. Results and discussion

As stated earlier, the SAR sensor satellites and InSAR technology for environmental monitoring and disaster management are presented. The results of earthquake-induced displacement modeling (i.e., based on the InSAR technology) after change detection modeling are provided and discussed here. In this section, to model ground movement in the study area triggered by the Sarpol-e Zahab earthquake on 25th November 2018, the InSAR Interferogram of surface deformation is created and discussed.

3.1 SARPROZ analysis

A SAR signal has phase and amplitude information where the phase is the fraction of one complete sine wave cycle, and the amplitude is the strength of the radar response. The phase of the SAR image is determined by the distance between the ground targets and the satellite antenna. InSAR uses the phase difference between two sophisticated radar SAR observations with a slightly different sensor position. An interferogram is created by a combination of the phase of these two images after co-registration, whose phase is linked to the terrain topography. In the interferogram, one image is defined as a master image, while the other image is a slave image. The interferogram is constructed by cross multiplying the master image with the complex conjugate of the slave. While the phase is the phase difference between the two images, the amplitude of both images is multiplied. The interferometric phase of each SAR image pixel is linked only with travel paths differences from each of the two SARs to the interested resolution cell. The interferometric phase variation $d\emptyset$ is then proportional to dR divided by the transmitted wavelength λ (Eqs. (1) to (3)). In the interferogram, the interferometric phase is ambiguous and only known within 2π. To link the interferometric phase to the topographic height, the phase should be unwrapped. Phase unwrapping solves the ambiguity by integrating the phase difference between neighboring pixels. Unwrapped results should be considered as a relative displacement/ height/between two pixels (European Space Agency 2016).

$$\emptyset_1 = \frac{4\pi R}{\lambda} \tag{1}$$

$$\emptyset_2 = \frac{4\pi (R + dR)}{\lambda} \tag{2}$$

$$d\emptyset = \emptyset_2 - \emptyset_1 = \frac{4\pi dR}{\lambda} \tag{3}$$

With the use of SAR interferometry, geometric information is extracted from conjugated complex multiplication of Master and Slave images, which have slightly different sensor positions where it gives 3D positions of scattering elements. With the use of external DEM, deformation values are extracted besides the estimation of topography. The restriction of InSAR would be where coherence is decreasing, and InSAR is not practical. The issue rises where several persistent scatter points are not affected by the properties of spatial-temporal variation of backscattering. This restriction is solved by long-term monitoring for surface deformation extraction. Soil moisture and vegetation information are obtained from coherence and intensity values.

Interferogram of surface deformation (see Fig. 5) after the earthquake occurred in Sarpol-e Zahab on 25th November 2018 is created where Digital Elevation Model (DEM) is removed in topographic phase removal by subtracting the reference DEM (SRTM 3 second) from the interferogram. Noise from temporal decorrelation, geometric decorrelation, volume scattering, and processing error can corrupt the interferometric phase, which is needed to be removed. In this study, Goldstein phase filtering with an empirical window size of 15 by 15 is used to increase the signal-to-noise ratio as interferogram phase filtering. For unwrapping the interferogram and converting it as

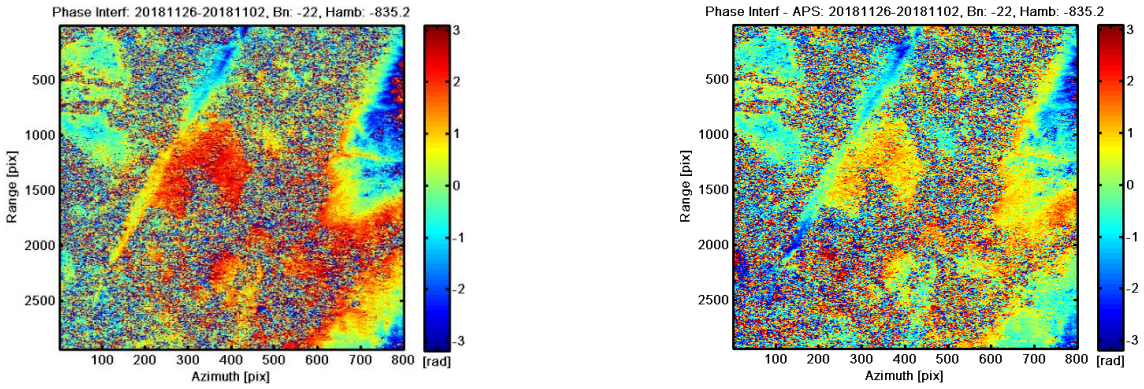

(a) (b)

Fig. 5 (a) Interferogram of surface deformation (left image); (b) atmospherically corrected interferogram (right image) after the earthquake in Sarpol-e Zahab on 25th November 2018 processed in SARPROZ in MATLAB

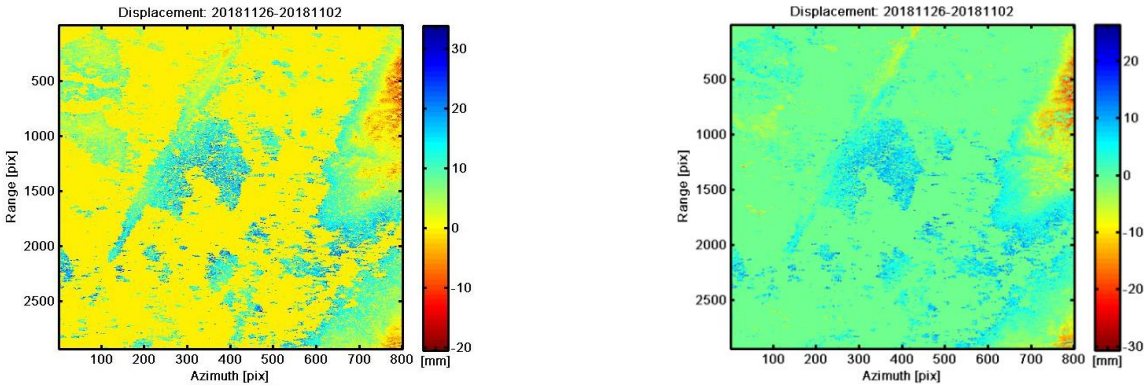

(a) (b)

Fig. 6 (a) Displacement image (left image); (b) atmospheric corrected displacement image (right image) of the Sarpol-e Zahab due to the earthquake on 25th November 2018.

a displacement map in millimeter using SARPROZ in MATLAB programing language on HP Spectre with an Intel Core-i5 system with 8-GB RAM., sparse least square with coherence image as the mask image with an empirical threshold of 0.3 is used. Fig. 6 presents displacement images caused by the Sarpol-e Zahab earthquake in Kermanshah, western Iran. Atmospheric Phase Screen (APS) is required to be removed or reduced from the interferogram image. APS depends on local temperature, humidity, and pressure. In this research, for correcting APS, long spatial wavelengths are masked and removed. Long wavelengths were considered as atmospheric delay, and they were removed from interferograms (see Figs. 5(b) and 6(b)). For a better estimation of APS, six SLC images of Sarpol-e Zahab region are used.

Results of InSAR modeling show that there is a vertical ground movement between -7 millimeters to +18 millimeters in the study area after the Sarpol-e Zahab earthquake (see Fig. 7). Mean, minimum, maximum, median values of ground movement are equal to +2 mm, -7 mm, +18 mm, +2 mm, respectively.

Peak Ground Acceleration (PGA) (see Fig. 7(c)) and Peak Ground Velocity (PGV) (see Fig. 7(d)) can be used for potential damage defined by the United States Geological survey. PGV presents the most significant value of how fast a ground point is shaking due to an earthquake at a particular location. PGA shows the most considerable amount in increasing the velocity, which is recorded at a specific station during an earthquake. Ground motion is related to buildings and infrastructure damage due to an earthquake, so basically, both PGA and PGV are relevant and accurate metrics to determine how an earthquake may results in small or massive damages to buildings near the earthquake location. 2018 Sarpol-e Zahab earthquake had a peak ground acceleration from 0.2 to 0.24, which is considered as type VII with a moderate potential of damage. 2018 Sarpol-e Zahab earthquake had a peak ground velocity from 12 to 18 that is regarded as types VI and VII with light and average possibilities of contamination (see Table 2) (the data is freely available at https://earthquake.usgs.gov).

Out of 682 damaged buildings and infrastructures due to the 2017 Sarpol-e Zahab earthquake (see Fig. 7(a)), 574 structures are moved from -2 to +17 mm (see Figs. 7(b) and 8). Even though the displacements are small, but it can be harmful to damaged infrastructures. Based on this research, damaged buildings and infrastructures should be checked for further possible new damages caused by the 2018 Sarpol-e Zahab earthquake, especially building related to gas and water stations. The presented results can be useful for likely new damaged buildings or infrastructures for

Table 2 Peak ground acceleration and velocity potential damage according to United States Geological Survey

Instrumental intensity	Acceleration (g)	Velocity (cm/s)	Perceived shaking	Potential damage
I	< 0.0017	< 0.1	Not felt	None
II–III	0.0017– 0.014	0.1 – 1.1	Weak	None
IV	0.014 – 0.039	1.1 – 3.4	Light	None
V	0.039 – 0.092	3.4 – 8.1	Moderate	Very light
VI	0.092 – 0.18	8.1 – 16	Strong	Light
VII	0.18 – 0.34	16 – 31	Very strong	Moderate
VIII	0.34 – 0.65	31 – 60	Severe	Moderate to heavy
IX	0.65 – 1.24	60 – 116	Violent	Heavy
X+	> 1.24	> 116	Extreme	Very heavy

agencies such as municipalities for further investigation.

As presented in Fig. 9, regions with a higher altitude, which are mountainous areas, suffered subsidence with negative values where urban areas with lower height experienced ground uplift (heave) with positive values. Vegetation and farm areas had the least ground displacement.

3.2 Validation of the result

At 21:48' (local time), on November 12, 2017, a strong quake of magnitude 7.3 struck the region west of Kermanshah city (within Zagros structural domain), in western Iran. The death toll in this event has risen to at least 400. The powerful earthquake caused vast destruction in the region, given the number of cities and villages located within the affected area (see Fig. 10).

The affected zone of this great seismic event contains the MFF (Mountain Front Fault) and HZF (High Zagros Fault) of the main Zagros structures. Within the study area, these two active fault zones are located closer to each other in the NW. In the Zagros structural domain, the MFF is a basement thrust fault (dipping NE), and the HZF is a reverse fault with a small dextral component (dipping NE). The assessment was mainly focused on the Sarpol-e Zahab region and Ezgaleh city due to the extent of destruction and that being relatively close to the source of the earthquake (MFF and HFZ). Our preliminary assessment highlights the concentration of the secondary order co-seismic geological features on the hanging wall of the MFF, close to the HZF zone.

In general view, most of the Zagros active thrust faults

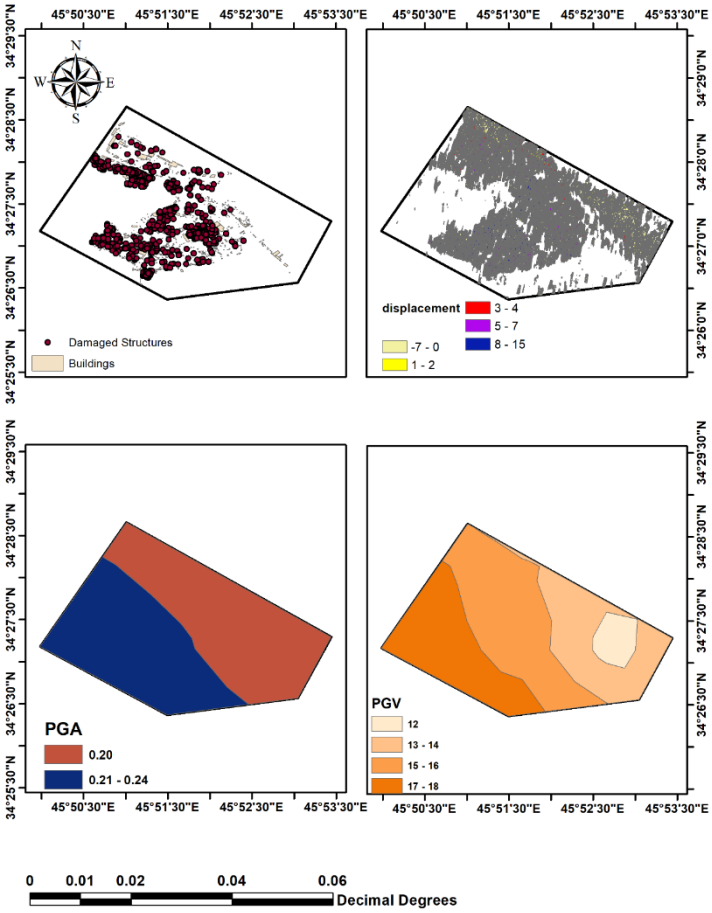

Fig. 7 (a) Damaged structures after the 2017 earthquake; (b) displacement map of Sarpol-e Zahab after the 2018 earthquake in millimeters; (c) peak ground acceleration due to the 2018 earthquake in g; (d) peak ground velocity due to the 2018 earthquake in cm/s

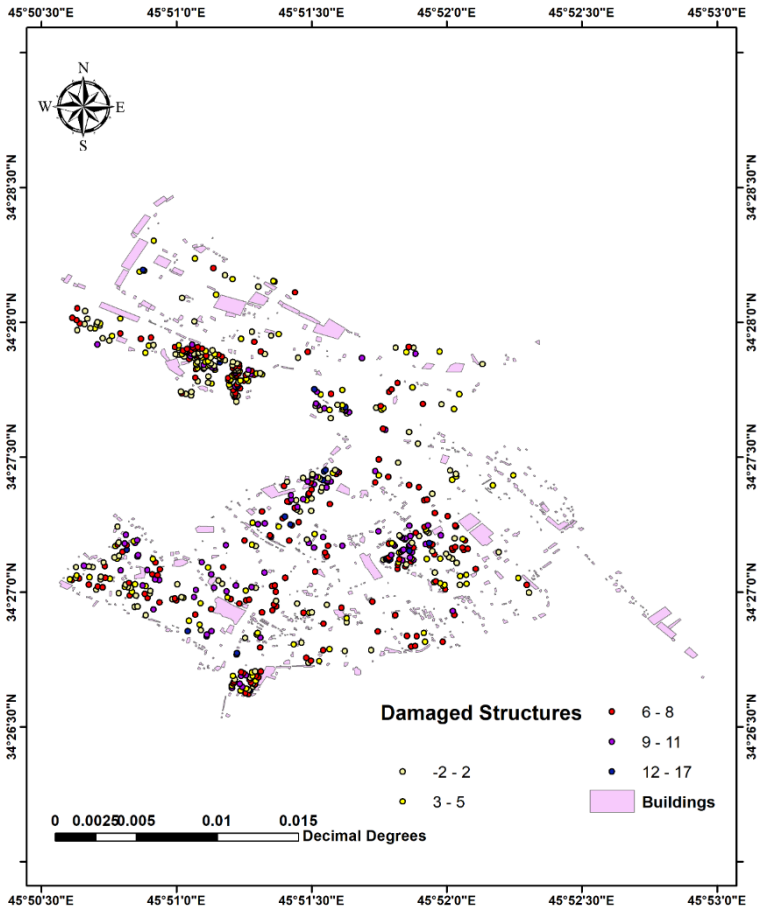

Fig. 8 Damaged structures (due to the 2017 Sarpol-e Zahab earthquake) that have moved due to the 2018 Sarpol-e Zahab earthquake

play a role as blind faults (e.g., Berberian 1995). However, taking into account the magnitude of the earthquake occurred at a shallow depth, there could be a possibility of forming a co-seismic surface faulting. The recent studies (e.g., Motaghi *et al*. (2017); Karimzadeh *et al*. (2018)) reveal the detachment depth of 15-18 km in the basement within this sector of the Zagros domain. This is more or less in agreement with the focal depth of the recent earthquake. Hence, it is possible for the quake not to be accompanied by surface faulting. In several zones, landslides were triggered by the 2017 earthquake, including Meleh-kabood and north Dalaho landslides (see Figs. 11 and 12).

Considering that there are several landslide zones (e.g., Meleh-Kabood landslide) near the study area caused by the 2017 earthquake, As shown in Fig. 13, 2018 Sarpol-e Zahab earthquake triggered another ground movement in the study area where most of Sarpol-e Zahab buildings are moved.

The displacement map shows vertical movement where negative values present ground subsidence and positive values present heave. As seen as in the unwrapped phase of the Sarpol-e Zahab region, the city suffered heave (uplift) up to 18 mm and subsidence up to -8 mm after the 2018 earthquake. Sarpol-e Zahab city was suffering ground subsidence before the 2018 earthquake. 2018 Sarpol-e Zahab earthquake reversed the ground movement from subsidence to heave (see Fig. 14). For tracking the surface deformation before the 2018 earthquake, first, the unwrapped phase from 9th October 2018 to 2nd November 2018 is modeled which shows that the area was suffering from land subsidence and then the unwrapped phase from 2nd November 2018 to 26th November 2018 is modeled which show that the 2018 earthquake has reversed the land movement for the time frame.

In this study, suitable parameters and filters for creating interferogram and APS estimation are selected experimentally. Two factors are considered to check the suitability and accuracy of selected parameters and filter, including temporal coherence and phase residual. Phase residual should be small if parameters are chosen correctly (see Fig. 15(a)). On the other hand, selected parameters and filters are suitable if temporal coherence is close to 1 (see Fig. 15(b)). Phase residual is the phase minus estimated APS and other estimated parameters. Both factors can be used as a tool for recognizing the accuracy of the results, including interferogram and displacement map. It should be considered that different parameters are experimentally selected, and with the least values for phase residuals and the most values close to one for temporal coherence, the final parameters are selected for this study. In the temporal coherence map, values of 1 present that there is no error in the estimation of the unwrapped phase where the values less than 1 show that error is present in the estimated unwrapped phase.

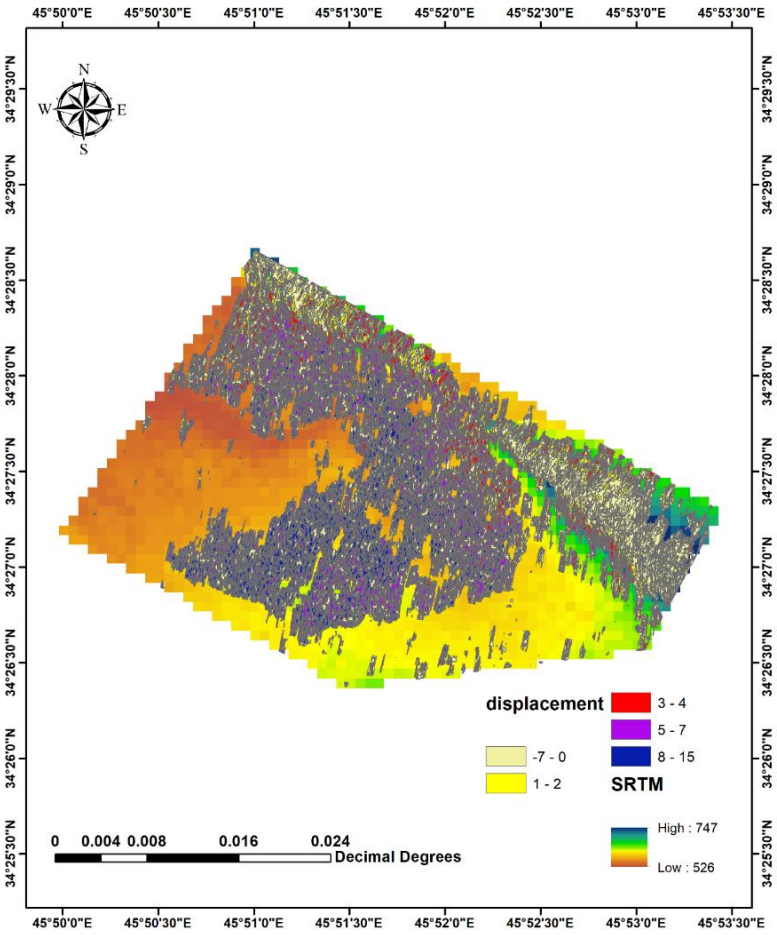

Fig. 9 Displacement map of the 2018 Sarpol-e Zahab earthquake with Digital Elevation Map in millimeters

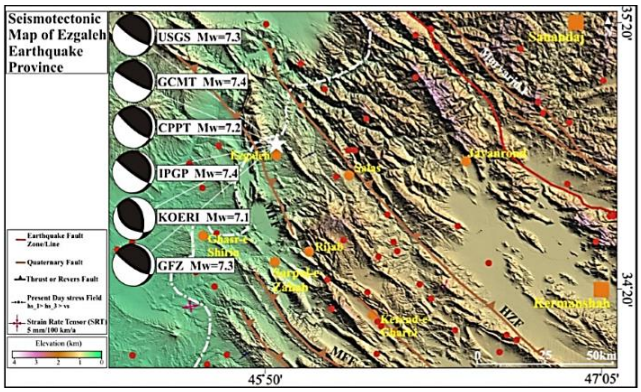

Fig. 10 The domain of the West Kermanshah-Ezgaleh earthquake presented in the seismotectonic map of the area. Epicenter from IIEES

4. Conclusions

Downward and upward movement of the ground's surface caused by an earthquake is called land subsidence and uplift, respectively. Both land subsidence and land uplift as ground deformation on a large scale are identifiable with InSAR technology, which can be used for geophysics, geohazards, and geology applications. For ubran subsidence and infrastructure monitoring, InSAR is a useful tool for researchers, private and public agencies, wherein

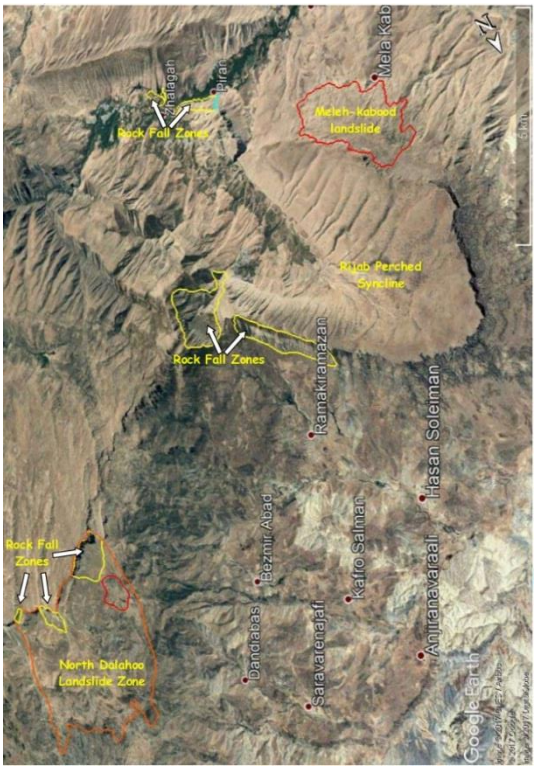

Fig. 11 Several landslide zones triggered by the 2017 earthquake

Fig. 12 Monitoring of the land movement in the study area due to the 2017 earthquake (Meleh-Kabood mass movement)

this study movement of damaged buildings and infrastructures by the 2017 Sarpol-e Zahab earthquake, due to the 2018 earthquake were investigated. In the study area, a devastating earthquake in 2017 with a magnitude of 6.3 Richter triggered several landslides and rockfalls which were studied. In this research, the use of the SAR data of Sentinel 1A SLC in a case study belonging to 25th November 2018 Ms 6.3 Sarpol-e Zahab earthquake, Kermanshah province of Iran. For displacement modeling caused by this disaster, InSAR technology is used.

Regarding previously-one researches, the SAR implies a capable method for monitoring the surface deformations, usually caused by seismic, tectonic, and volcanic activity, slope failure, ice and rock glacier motion, and subsidence induced by groundwater pumping, hydrocarbon extraction, mining, and natural compaction. In comparison with point-wise evaluative techniques such as GPS and leveling, the main superiority of SAR lies in two-dimensional spatial coverage. This is a while; decorrelation can be mentioned as a problem of SAR interferometry. Changing the scatterer characteristics causes temporal decorrelation. Results of InSAR shows that almost all area of the Sarpol-e Zahab ground, particularly the forest region on the steep slopes has been moved within a range of -7 mm to +18 mm. The results of this research are useful for the private and public sectors such as Sarpol-e Zahab municipality for the identification of damaged buildings and infrastructures that are moved by the 2018 Sarpol-e Zahab earthquake. This information would be vital where possible broken water and gas stations could be recognized, and further investigation by the responsible sectors would be of interest. Results show that the 2018 earthquake has reversed land subsidence in urban areas caused by the 2017 earthquake, and those urban areas are suffering land uplift afterward.

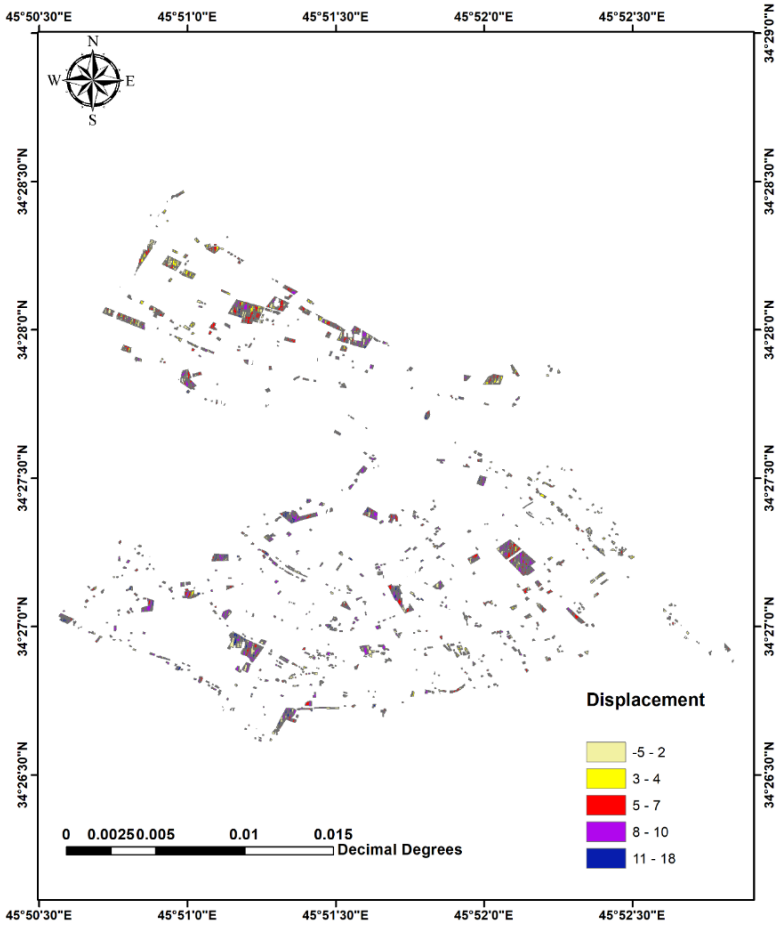

Fig. 13 Displace map of Sarpol-e Zahab buildings after the 2018 Sarpol-e Zahab earthquake in millimeters

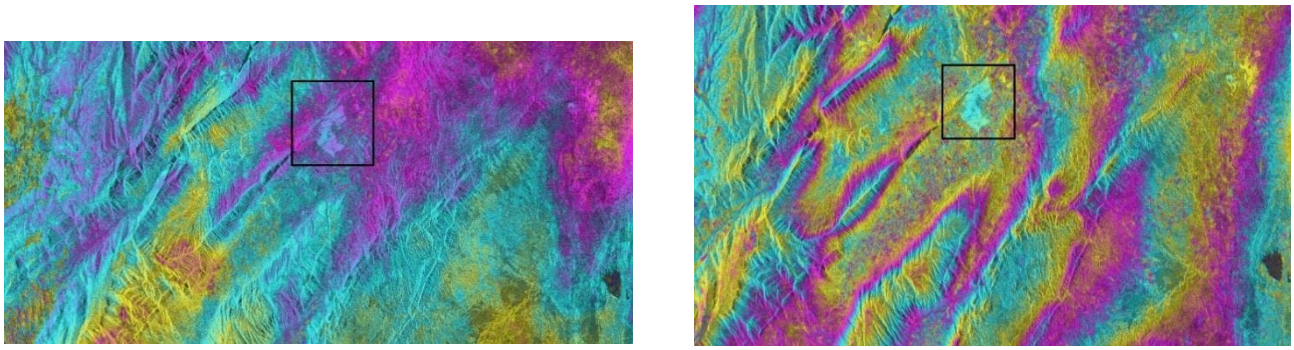

(a) (b)

Fig. 14 (a) The unwrapped phase of the region before the 2018 Sarpol-e Zahab earthquake (top image, from 9th October 2018 to 2nd November 2018); (b) The unwrapped period of the area after the 2018 Sarpol-e Zahab earthquake (down the image, from 2nd November 2018 to 26th November 2018)

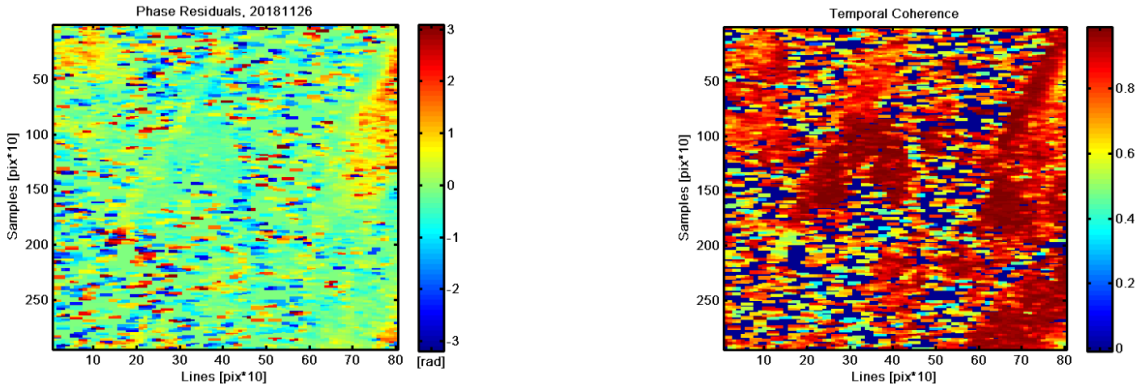

(a) (b)

Fig. 15 (a) Phase residual (up image); (b) temporal coherence (down image)

Conflicts of Interest

The authors declare no conflict of interest.

References

Agard, P., Omrani, J., Jolivet, L. and Mouthereau, F. (2005), "Convergence history across Zagros (Iran): constraints from collisional and earlier deformation", *Int. J. Earth Sci.*, **94**(3), 401-419. https://doi.org/10.1007/s00531-005-0481-4

Barnhart, W.D., Brengman, C.M., Li, S. and Peterson, K.E. (2018), "Ramp-flat basement structures of the Zagros Mountains inferred from co-seismic slip and afterslip of the 2017 Mw7.3 Darbandikhan, Iran/Iraq earthquake", *Earth Planet. Sci. Lett.*, **496**, 96-107. https://doi.org/10.1016/j.epsl.2018.05.036

Baziar, M.H. and Rostami, H. (2017), "Earthquake demand energy attenuation model for liquefaction potential assessment", *Earthq. Spectra*, **33**(2), 757-780. https://doi.org/10.1193/030816eqs037m

Berardino, P., Fornaro, G., Lanari, R. and Sansosti, E. (2002), "A new algorithm for surface deformation monitoring based on small baseline differential SAR interferograms", *IEEE Transact. Geosci. Remote Sensing*, **40**(11), 2375-2383. https://doi.org/10.1109/TGRS.2002.803792

Berberian, M. (1995), "Master "blind" thrust faults hidden under the Zagros folds: active basement tectonics and surface morphotectonics", *Tectonophysics*, **241**(3-4), 193-224. https://doi.org/10.1016/0040-1951(94)00185-C

Bui, D.T., Moayedi, H., Gör, M., Jaafari, A. and Foong, L.K. (2019a), "Predicting slope stability failure through machine learning paradigms", *ISPRS Int. J. Geo-Inform.*, **8**(9), 395. https://doi.org/10.3390/ijgi8090395

Bui, D.T., Moayedi, H., Kalantar, B., Osouli, A., Gör, M., Pradhan, B., Nguyen, H. and Rashid, A.S.A. (2019b), "Harris hawks optimization: A novel swarm intelligence technique for spatial assessment of landslide susceptibility", *Sensors*, **19**, 3590.

Bui, D.T., Moayedi, H., Kalantar, B., Osouli, A., Pradhan, B., Nguyen, H. and Rashid, A.S.A. (2019c), "A novel swarm intelligence—Harris hawks optimization for spatial assessment of landslide susceptibility", *Sensors*, **19**(16), 3590. https://doi.org/10.3390/s19163590

Chen, Q., Cheng, H., Yang, Y., Liu, G. and Liu, L. (2014), "Quantification of mass wasting volume associated with the giant landslide Daguangbao induced by the 2008 Wenchuan earthquake from persistent scatterer InSAR", *Remote Sens. Environ.*, **152**, 125-135. https://doi.org/10.1016/j.rse.2014.06.002

Chen, H., Zhang, Q., Luo, J., Xu, Y. and Zhang, X. (2020), "An enhanced Bacterial Foraging Optimization and its application for training kernel extreme learning machine", *Appl. Soft Comput.*, **86**, 105884. https://doi.org/10.1016/j.asoc.2019.105884

Choi, J.C., Lee, S.R., Kim, Y. and Song, Y.H. (2011), "Real-time unsaturated slope reliability assessment considering variations in monitored matric suction", *Smart Struct. Syst., Int. J.*, **7**(4), 263-274. https://doi.org/10.12989/sss.2011.7.4.263

Dai, K., Li, Z., Tomás, R., Liu, G., Yu, B., Wang, X., Cheng, H., Chen, J. and Stockamp, J. (2016), "Monitoring activity at the Daguangbao mega-landslide (China) using Sentinel-1 TOPS time

series interferometry", *Remote Sens. Environ.*, **186**, 501-513. https://doi.org/10.1016/j.rse.2016.09.009

Debella-Gilo, M. and Kääb, A. (2012), "Measurement of surface displacement and deformation of mass movements using least squares matching of repeat high resolution satellite and aerial images", *Remote Sensing*, **4**(1) 43-67. https://doi.org/10.3390/rs4010043

Dicelis, G., Assumpção, M., Kellogg, J., Pedraza, P. and Dias, F. (2016), "Estimating the 2008 Quetame (Colombia) earthquake source parameters from seismic data and InSAR measurements", *J. South Am. Earth Sci.*, **7**, 250-265. https://doi.org/10.1016/j.jsames.2016.09.011

Du, Y., Feng, G., Liu, L., Fu, H., Peng, X. and Wen, D. (2020), "Understanding Land Subsidence Along the Coastal Areas of Guangdong, China, by Analyzing Multi-Track MTInSAR Data", *Remote Sensing*, **12**(2) 299.
Du, Y., Feng, G., Liu, L., Fu, H., Peng, X. and Wen, D.

Ebrahimi, M., Moradi, A., Bejvani, M. and Tafreshi, M.D. (2016), "Application of STA/LTA Based on Cross-Correlation to Passive Seismic Data", *Proceedings of the 6th EAGE Workshop on Passive Seismic*, Muscat, Oman, January, pp. 1-5.

European Space Agency (2016), Interferometry Tutorial.

Fang, L., Xu, Y., Yao, W. and Stilla, U. (2016), "Estimation of glacier surface motion by robust phase correlation and point like features of SAR intensity images", *ISPRS J. Photogram. Remote Sensing*, **121**, 92-112. https://doi.org/10.1016/j.isprsjprs.2016.08.012

Farolfi, G., Piombino, A. and Catani, F. (2019), "Fusion of GNSS and Satellite Radar Interferometry: Determination of 3D Fine-Scale Map of Present-Day Surface Displacements in Italy as Expressions of Geodynamic Processes", *Remote Sensing*, **11**(4), 394. https://doi.org/10.3390/rs11040394

Ferretti, A., Prati, C. and Rocca, F. (1999), "Permanent scatterers in SAR interferometry", *Proceedings of IEEE 1999 International Geoscience and Remote Sensing Symposium*, *IGARSS'99*, (Cat. No.99CH36293), Vol.1523, pp. 1528-1530.

Glenn, N.F., Streutker, D.R., Chadwick, D.J., Thackray, G.D. and Dorsch, S.J. (2006), "Analysis of LiDAR-Derived Topographic Information for Characterizing and Differentiating Landslide Morphology and Activity", *Geomorphology*, **73**(1). https://doi.org/10.1016/j.geomorph.2005.07.006

Guha-Sapir, D., Vos, F., Below, R. and Ponserre, S. (2012), "Annual disaster statistical review 2011: the numbers and trends", In: Centre for Research on the Epidemiology of Disasters (CRED), C.f.R.o.t.E.o.D. (Ed.).

He, L., Tan, J., Hu, Q., He, S., Cai, Q., Fu, Y. and Tang, S. (2018), "Non-contact measurement of the surface displacement of a slope based on a smart binocular vision system", *Sensors*, **18**(9), 2890. https://doi.org/10.3390/s18092890

Hooper, A. (2008), "A multi-temporal InSAR method is incorporating both persistent scatterer and small baseline approaches", *Geophys. Res. Lett.*, **35**(16). https://doi.org/10.1029/2008GL034654

Hugenholtz, C.H., Whitehead, K., Brown, O.W., Barchyn, T.E., Moorman, B.J., LeClair, A., Riddell, K. and Hamilton, T. (2013), "Geomorphological mapping with a small unmanned aircraft system (sUAS): Feature detection and accuracy assessment of a photogrammetrically-derived digital terrain model", *Geomorphology*, **194**, 16-24. https://doi.org/10.1016/j.geomorph.2013.03.023

Jinlong, L., Wenjie, X., Jianjing, Z., Wei, L., Xilin, S. and Chunhe, Y. (2020), "Modeling the mining of energy storage salt caverns using a structural dynamic mesh", *Energy*, **193**, 116730. https://doi.org/10.1016/j.energy.2019.116730

Kargar, P., Osouli, A., Vaughn, B., Hosseini, A. and Rostami, H. (2020), "Feasibility Study of Collapse Remediation of Illinois Loess Using Electrokinetics Technique by Nanosilica and Salt", *Proceedings of Geo-Congress 2020*, *Foundations*, *Soil Improvement*, *and Erosion*, Reston, VA, USA, Febraury, pp. 667-675. https://doi.org/10.1061/9780784482780.066

Karimzadeh, S., Cakir, Z., Osmanoğlu, B., Schmalzle, G., Miyajima, M., Amiraslanzadeh, R. and Djamour, Y. (2013), "Interseismic strain accumulation across the North Tabriz Fault (NW Iran) deduced from InSAR time series", *J. Geodyn.*, **66**, 53-58. https://doi.org/10.1016/j.jog.2013.02.003

Karimzadeh, S., Matsuoka, M., Miyajima, M., Adriano, B., Fallahi, A. and Karashi, J. (2018), "Sequential SAR coherence method for the monitoring of buildings in Sarpole-Zahab, Iran", *Remote Sensing*, **10**(8), 1255. https://doi.org/10.3390/rs10081255

Kallel, A., Erguler, Z.A., Cui, Z.D., Karrech, A., Karakus, M., Kulatilake, P. and Shukla, S.K. (2019), *Recent Advances in Geo-Environmental Engineering*, *Geomechanics and Geotechnics*, *and Geohazards*, Springer, Cham, pp. 481-483.

Li, Z. and Bethel, J. (2008), "Image coregistration in SAR interferometry", *Int. Arch. Photogram. Remote Sens. Spatial Inform. Sci.*, **37**, 433-438.

Liu, W., Zhang, X., Li, H. and Chen, J. (2020), "Investigation on the deformation and strength characteristics of rock salt under different confining pressures", *Geotech. Geol. Eng.* https://doi.org/10.1007/s10706-020-01388-1

Mei, D.P. (2017), "Structural health monitoring-based dynamic behavior evaluation of a long-span high-speed railway bridge", *Smart Struct. Syst., Int. J.*, **20**(2), 197-205. https://doi.org/10.12989/sss.2017.20.2.197

Moayedi, H., Huat, B.B., Ali, T.A.M., Asadi, A., Moayedi, F. and Mokhberi, M. (2011), "Preventing landslides in times of rainfall: case study and FEM analyses", *Disaster Prev. Manage.: Int. J*, **20**(2), 115-124. https://doi.org/10.1108/09653561111126067

Moayedi, H., Mehrabi, M., Kalantar, B., Abdullahi Mu'azu, M.A., Rashid, A.S., Foong, L.K. and Nguyen, H. (2019a), "Novel hybrids of adaptive neuro-fuzzy inference system (ANFIS) with several metaheuristic algorithms for spatial hazard assessment of seismic-induced landslide", *Geomat. Natural Hazards Risk*, **10**(1), 1879-1911. https://doi.org/10.1080/19475705.2019.1650126

Moayedi, H., Mehrabi, M., Mosallanezhad, M., Rashid, A.S.A. and Pradhan, B. (2019b), "Modification of landslide susceptibility mapping using optimized PSO-ANN technique", *Eng. Comput.*, **35**(3), 967-984. https://doi.org/10.1007/s00366-018-0644-0

Moayedi, H., Osouli, A., Bui, D.T., Kok Foong, L., Nguyen, H. and Kalantar, B. (2019c), "Two novel neural-evolutionary predictive techniques of dragonfly algorithm (DA) and biogeography-based optimization (BBO) for landslide susceptibility analysis", *Geomat. Natural Hazards Risk*, **10**(1), 2429-2453. https://doi.org/10.1080/19475705.2019.1699608

Moayedi, H., Osouli, A., Tien Bui, D. and Foong, L.K. (2019d), "Spatial landslide susceptibility assessment based on novel neural-metaheuristic geographic information system based ensembles", *Sensors*, **19**(21), 4698. https://doi.org/10.3390/s19214698

Moayedi, H., Tien Bui, D. and Kok Foong, L. (2019e), "Slope stability monitoring using novel remote sensing based fuzzy logic", *Sensors*, **19**(21), 4636. https://doi.org/10.3390/s19214636

Montecino, H.D., de Freitas, S.R., Báez, J.C. and Ferreira, V.G. (2017), "Effects on Chilean Vertical Reference Frame due to the Maule Earthquake co-seismic and post-seismic effects", *J. Geodyn.*, **112**, 22-30. https://doi.org/10.1016/j.jog.2017.07.006

Motaghi, K., Shabanian, E. and Kalvandi, F. (2017), "Underplating along the northern portion of the Zagros suture zone, Iran", *Geophys. J. Int.*, **210**(1), 375-389. https://doi.org/10.1093/gji/ggx168

Nguyen, H., Mehrabi, M., Kalantar, B., Moayedi, H. and Abdullahi, M.A.M. (2019), "Potential of hybrid evolutionary approaches for assessment of geo-hazard landslide susceptibility

mapping", *Geomat. Natural Hazards Risk*, **10**(1), 1667-1693. https://doi.org/10.1080/19475705.2019.1607782

Oveisi, B., Lavé, J., Van Der Beek, P., Carcaillet, J., Benedetti, L. and Aubourg, C. (2009), "Thick-and thin-skinned deformation rates in the central Zagros simple folded zone (Iran) indicated by displacement of geomorphic surfaces", *Geophys. J. Int.*, **176**(2), 627-654. https://doi.org/10.1111/j.1365-246X.2008.04002.x

Pawluszek-Filipiak, K. and Borkowski, A. (2020), "Integration of DInSAR and SBAS Techniques to Determine Mining-Related Deformations Using Sentinel-1 Data: The Case Study of Rydułtowy Mine in Poland", *Remote Sensing*, **12**(2), 242. https://doi.org/10.3390/rs12020242

Perissin, D. (2019), SARPROZ Manual.

Qiao, W. and Yang, Z. (2019a), "Modified dolphin swarm algorithm based on chaotic maps for solving high-dimensional function optimization problems", *IEEE Access*, **7**, 110472-110486. https://doi.org/10.1109/ACCESS.2019.2931910

Qiao, W. and Yang, Z. (2019b), "Solving large-scale function optimization problem by using a new metaheuristic algorithm based on quantum dolphin swarm algorithm", *IEEE Access*, **7**, 138972-138989. https://doi.org/10.1109/ACCESS.2019.2942169

Qiao, W., Huang, K., Azimi, M. and Han, S. (2019a), "A novel hybrid prediction model for hourly gas consumption in supply side based on improved whale optimization algorithm and relevance vector machine", *IEEE Access*, **7**, 88218-88230. https://doi.org/10.1109/ACCESS.2019.2918156

Qiao, W., Tian, W., Tian, Y., Yang, Q., Wang, Y. and Zhang, J. (2019b), "The forecasting of PM2. 5 using a hybrid model based on wavelet transform and an improved deep learning algorithm", *IEEE Access*, **7**, 142814-142825. https://doi.org/10.1109/ACCESS.2019.2944755

Rostami, H., Baziar, M.H. and Alibolandi, M. (2018), "Reevaluation of SPT-Based Liquefaction Case History Using Earthquake Demand Energy", *Geotechnical Earthquake Engineering and Soil Dynamics V*: *Liquefaction Triggering*, *Consequences*, *and Mitigation*, Reston, VA, USA, pp. 493-501. https://doi.org/10.1061/9780784481455.047

Schumann, G.J.P. (2017), *Remote Sensing of Floods*, Oxford University Press.

Shen, L., Chen, H., Yu, Z., Kang, W., Zhang, B., Li, H., Yang, B. and Liu, D. (2016), "Evolving support vector machines using fruit fly optimization for medical data classification", *Knowledge-Based Syst.*, **96**, 61-75. https://doi.org/10.1016/j.knosys.2016.01.002

Shi, X., Zhang, L., Zhong, Y., Zhang, L. and Liao, M. (2020), "Detection and characterization of active slope deformations with Sentinel-1 InSAR analyses in the Southwest Area of Shanxi, China", *Remote Sensing*, **12**(3), 392. https://doi.org/10.3390/rs12030392

Stumpf, A. and Kerle, N. (2011), "Object-oriented mapping of landslides using Random Forests", *Remote Sens. Environ.*, **115**(10), 2564-2577. https://doi.org/10.1016/j.rse.2011.05.013

Taleshi, A.A., Arab-Amiri, A., Ebrahimi, M. and Abbasinia, M. (2016b), "Two and three-dimonsional ERT modelling for a buried tunnel", *J. Emerg. Trends Eng. Appl. Sci.*, **7**(3), 118-127.

Tsai, T.L. and Chen, H.F. (2010), "Effects of degree of saturation on shallow landslides triggered by rainfall", *Environ. Earth Sci.*, **59**(6), 1285-1295. https://doi.org/10.1007/s12665-009-0116-3

Valerio, E., Tizzani, P., Carminati, E., Doglioni, C., Pepe, S., Petricca, P., De Luca, C., Bignami, C., Solaro, G., Castaldo, R. and De Novellis, V. (2018), "Ground Deformation and Source Geometry of the 30 October 2016 Mw 6.5 Norcia Earthquake (Central Italy) Investigated Through Seismological Data, DInSAR Measurements, and Numerical Modelling", *Remote Sensing*, **10**(12), 1901. https://doi.org/10.3390/rs10121901

Van Dao, D., Jaafari, A., Bayat, M., Mafi-Gholami, D., Qi, C., Moayedi, H., Van Phong, T., Ly, H.B., Le, T.T., Trinh, P.T. and Luu, C. (2020), "A spatially explicit deep learning neural network model for the prediction of landslide susceptibility", *CATENA*, **188**, 104451. https://doi.org/10.1016/j.catena.2019.104451

Vernant, P., Nilforoushan, F., Hatzfeld, D., Abbassi, M.R., Vigny, C., Masson, F., Nankali, H., Martinod, J., Ashtiani, A., Bayer, R. and Tavakoli, F. (2004), "Present-day crustal deformation and plate kinematics in the Middle East constrained by GPS measurements in Iran and northern Oman", *Geophys. J. Int.*, **157**(1), 381-398. https://doi.org/10.1111/j.1365-246X.2004.02222.x

Wang, M. and Chen, H. (2020), "Chaotic multi-swarm whale optimizer boosted support vector machine for medical diagnosis", *Appl. Soft Comput.*, **88**, 105946. https://doi.org/10.1016/j.asoc.2019.105946

Wang, M., Chen, H., Yang, B., Zhao, X., Hu, L., Cai, Z., Huang, H. and Tong, C. (2017), "Toward an optimal kernel extreme learning machine using a chaotic moth-flame optimization strategy with applications in medical diagnoses", *Neurocomputing*, **267**, 69-84. https://doi.org/10.1016/j.neucom.2017.04.060

Wang, B., Zhao, C., Zhang, Q. and Peng, M. (2019), "Sequential InSAR Time Series Deformation Monitoring of Land Subsidence and Rebound in Xi'an, China", *Remote Sensing*, **11**(23), 2854. https://doi.org/10.3390/rs11232854

Wang, H., Moayedi, H. and Foong, L.K. (2020), "Genetic algorithm hybridized with multilayer perceptron to have an economical slope stability design", *Eng. Comput.*, 1-12. https://doi.org/10.1007/s00366-020-00957-5

Wright, T.J., Parsons, B.E. and Lu, Z. (2004), "Toward mapping surface deformation in three dimensions using InSAR", *Geophys. Res. Lett.*, **31**(1). https://doi.org/10.1029/2003GL018827

Xu, X. and Chen, H.-L. (2014), "Adaptive computational chemotaxis based on field in bacterial foraging optimization", *Soft Computing*, **18**(4), 797-807. https://doi.org/10.1007/s00500-013-1089-4

Xu, Y., Chen, H., Luo, J., Zhang, Q., Jiao, S. and Zhang, X. (2019), "Enhanced Moth-flame optimizer with mutation strategy for global optimization", *Inform. Sci.*, **492**, 181-203. https://doi.org/10.1016/j.ins.2019.04.022

Yang, Y.J., Hwang, C., Hung, W.C., Fuhrmann, T., Chen, Y.A. and Wei, S.H. (2019), "Surface deformation from sentinel-1A InSAR: Relation to seasonal groundwater extraction and rainfall in central Taiwan", *Remote Sensing*, **11**(23), 2817. https://doi.org/10.3390/rs11232817

Yuan, C. and Moayedi, H. (2019a), "Evaluation and comparison of the advanced metaheuristic and conventional machine learning methods for prediction of landslide occurrence", *Eng. Comput*, **36**, 1-11. https://doi.org/10.1007/s00366-019-00798-x

Yuan, C. and Moayedi, H. (2019b), "Evaluation and comparison of the advanced metaheuristic and conventional machine learning methods for the prediction of landslide occurrence", *Eng Comput.*, 1-11. https://doi.org/10.1007/s00366-019-00798-x

Zhang, C.C., Zhu, H.H., Shi, B., She, J.K. and Zhang, D. (2016), "Performance evaluation of soil-embedded plastic optical fiber sensors for geotechnical monitoring", *Smart Struct. Syst., Int. J.*, **17**(2), 297-311. https://doi.org/10.12989/sss.2016.17.2.297

Zhang, T., Shen, W.B., Wu, W., Zhang, B. and Pan, Y. (2019a), "Recent surface deformation in the Tianjin area revealed by Sentinel-1A data", *Remote Sensing*, **11**(2), 130. https://doi.org/10.3390/rs11020130

Zhang, Z., Jiang, D., Liu, W., Chen, J., Li, E., Fan, J. and Xie, K. (2019b), "Study on the mechanism of roof collapse and leakage of horizontal cavern in thinly bedded salt rocks", *Environ. Earth Sci.*, **78**(10), 292. https://doi.org/10.1007/s12665-019-8292-2

Zhou, G., Moayedi, H., Bahiraei, M. and Lyu, Z. (2020a),

"Employing artificial bee colony and particle swarm techniques for optimizing a neural network in prediction of heating and cooling loads of residential buildings", *J. Cleaner Prod*., **254**. https://doi.org/10.1016/j.jclepro.2020.120082

Zhou, G., Moayedi, H. and Foong, L.K. (2020b), "Teaching–learning-based metaheuristic scheme for modifying neural computing in appraising energy performance of building", *Eng. Comput*., **36**. https://doi.org/10.1007/s00366-020-00981-5

Zhu, H.H., Ho, A.N., Yin, J.H., Sun, H.W., Pei, H.F. and Hong, C.Y. (2012), "An optical fibre monitoring system for evaluating the performance of a soil nailed slope", *Smart Struct. Syst*., *Int. J*., **9**(5), 393-410. https://doi.org/10.12989/sss.2012.9.5.393

CC